LAWRENCE
LIVERMORE
NATIONAL
LABORATORY

UCRL-CONF-235728

DIELECTRIC WALL ACCELERATOR TECHNOLOGY

S. Sampayan, G. Caporaso, Y-J. Chen, J. Harris, S. Hawkins, C. Holmes, S. Nelson, B. Poole, M. Rhodes, D. Sanders, J. Sullivan, L. Wang, J. Watson

October 23, 2007

Pulsed Power Conference
Albuquerque, NM, United States
June 18, 2007 through June 22, 2007

Disclaimer

DIELECTRIC WALL ACCELERATOR TECHNOLOGY*

S. Sampayan, G. Caporaso, Y-J. Chen, J. Harris, S. Hawkins, C. Holmes, S. Nelson, B. Poole, M. Rhodes, D. Sanders, J. Sullivan, L. Wang and J. Watson

Beam Research Program
Lawrence Livermore National Laboratory
P.O. Box 808, L-645
Livermore, CA 94551

Abstract

The dielectric wall accelerator (DWA) is a compact pulsed power device where the pulse forming lines, switching, and vacuum wall are integrated into a single compact geometry. For this effort, we initiated a extensive compact pulsed power development program and have pursued the study of switching (gas, oil, laser induced surface flashover and photoconductive), dielectrics (ceramics and nanoparticle composites), pulse forming line topologies (asymmetric and symmetric Blumleins and zero integral pulse forming lines), and multilayered vacuum insulator (HGI) technology. Finally, we fabricated an accelerator cell for test on ETA-II (a 5.5 MeV, 2 kA, 70 ns pulsewidth electron beam accelerator). We review our past results and report on the progress of accelerator cell testing.

I. INTRODUCTION

We reported on compact accelerator technology being developed for radiography at Lawrence Livermore National Laboratory. This effort, funded in part under the US Department of Energy, has as its objective the production of a 20-30 ns, 2 kA electron beam pulse at a 10-20 MV/m gradient for portable radiography applications. Successfully meeting such objectives would allow the implementation of an equivalent FXR or DARHT accelerator in a 1-2 meter length structure at a projected cost of less than $2500/cm exclusive of the existing development program.

Ultra short pulse variants of this technology for use in cancer therapy and luggage interrogation have also been reported. In these configurations (Fig. 1 and 2), we use a pulsed ion source and configure the transmission lines for 1-10 ns pulses to take advantage of the increased surface flashover threshold at decreased pulse widths. Further, for extremely short pulses (~1 ns), the accelerator is configured in a traveling wave mode where the dielectric wall is excited along a small portion of the accelerator equivalent to the bunched length of particles.

Our near term prototype goal is based on oil switching. Although well proven, it is inadequate for high-repetition rate switching and high reliability commercial applications. As a long term development technology, we are also pursuing linear SiC photoconductive switching. This technology shows essentially instantaneous recovery and would allow MHz repetition rates within a burst. Such capability would allow a multiframe radiography capability in a compact and inexpensive package. In addition, such technology would be necessary in high reliability systems for continuous applications.

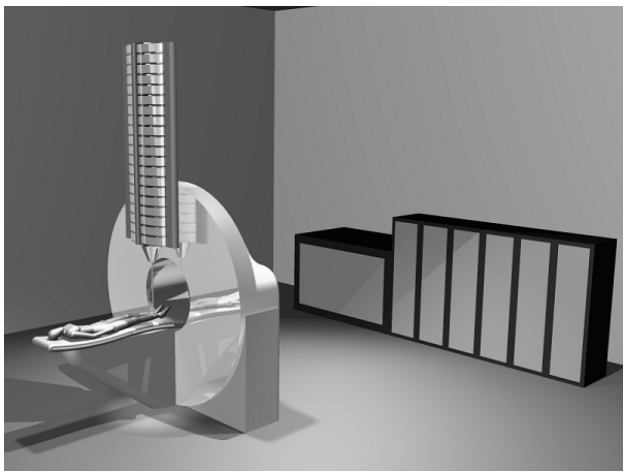

Figure 1 - Artist rendition of a 250 MeV cancer therapy system.

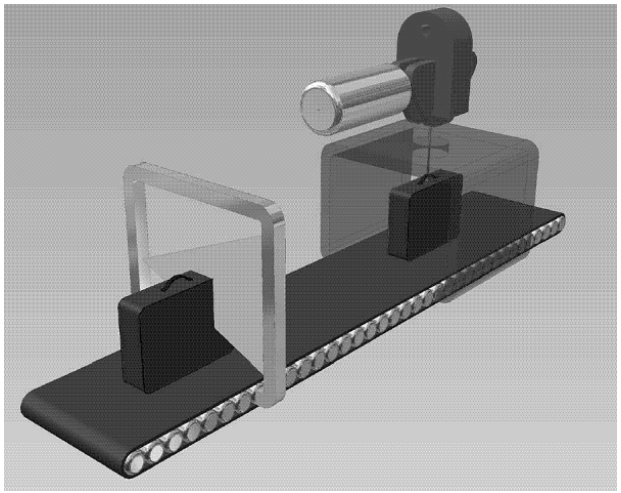

Figure 2 - High speed pixelized CT pre-screener (left) and post verifier (right) concept.

II. CELL DEVELOPMENT

A DWA prototype cell was designed and built for testing on ETA-II (a 5.5 MeV, 2.0 kA induction LINAC) In the following section, we survey the development of the cell components.

A. Oil Discharge and Photoconductive Switching

Previously, we reported on high pressure gas spark gaps as the means for switching the accelerator. Less than 1 ns simultaneity was demonstrated, but short resistive phase time and low inductance was difficult to achieve under the required constraints. Oil switching was subsequently selected because of the increased switch gradient capability and the resultant faster closure time.

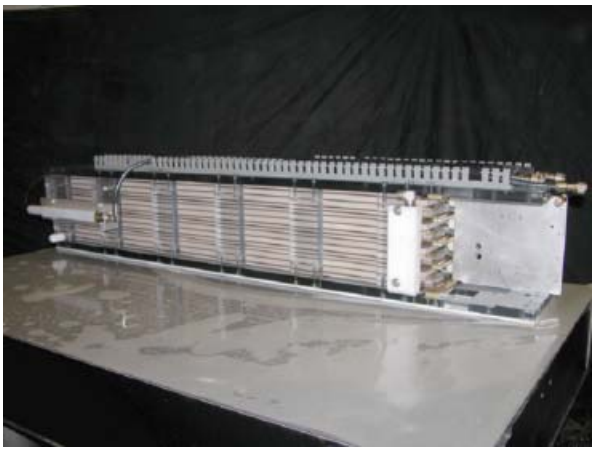

Figure 3. Oil switched four-stack Blumlein.

Switch testing was performed in a four stack Duroid based Blumlein system (Fig. 3). The system is pulsed-charged and each switch is used in the self-break mode. The particular geometry that proved the most successful was a short rail structure using copper electrodes (Fig. 4).

Jitter performance was 1.4 ns for a stack of four Blumleins as indicated by the break on the charging waveforms. Fast closure times also resulted in the erection of the voltage on the output (Fig. 5).

For commercialization and potential high rep-rate applications, we are also pursuing wide bandgap photoconductive switching (PCSS). Although a developmental technology, these materials have multiple advantages over conventional Si and GaAs technology. In particular, 6H-SiC and 2H-GaN (band-gaps ~3 – 3.4 eV), have high critical field strength (300-400 MV/m), high thermal conductivity, high-saturated electron velocity ($2.0 – 2.5x10^7$ cm/s) and sufficient carrier density ($\sim 10^{16} – 10^{17}/cm^3$) to achieve sub-ohm "on" resistance.

We reported on initial work in this area in our previous paper where we demonstrated the switch capability at 27 MV/m gradient. In that data, the photocurrent essentially followed the laser pulse temporal profile, demonstrating the high recovery rate of the material under high voltage conditions. Our more recent work has focused on measurement of the absorption properties at selected wavelengths, optical switching properties, and achieving higher electric field gradients across the substrate.

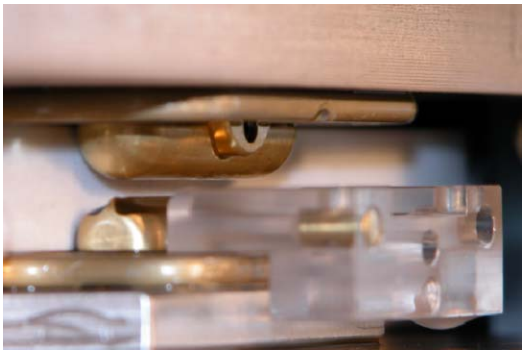

Figure 4. Blumlein oil switch.

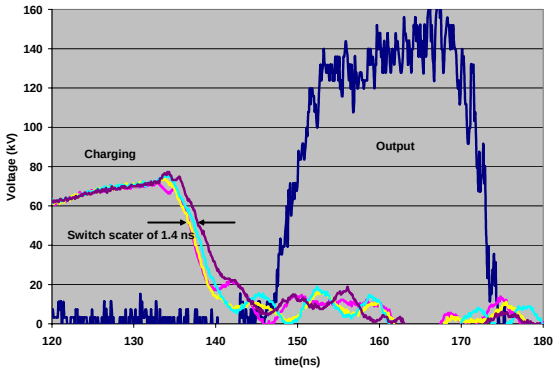

Figure 5. Demonstrated switch jitter (1.4 ns) and four stack Blumlein output.

The cause of the failure at 27 MV/m gradient in our previous work resulted from the discontinuity at the triple junction (i.e., the electrode-substrate-oil junction). In this first proof of concept test, little effort was spent optimizing the high voltage design. Systematic analysis of that region, however, showed a large enhancement (~ x10) thus demonstrating the capability of the material at ~300 MV/m (Fig. 6).

To realize the full capability of the material, we are developing techniques to better manage the enhanced electric field at that junction. Two of the techniques we are pursuing are shown in Figures 7 and 8.

In Figure 7, a cavity is formed in the substrate with a silicon oxide cap. This cavity receives the electrode and the electric field enhancement is graded in the vicinity.

An alternate technique of managing the electric fields is shown in Figure 8. With this particular method, a buried nitride layer is formed below the surface to act as a guard ring near the electrode triple junction.

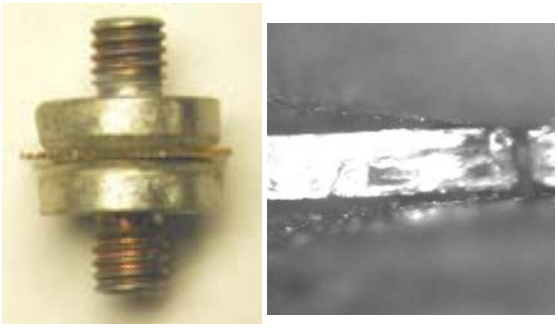

Figure 6. Proof of concept switch (left). Cross section of failure at the triple junction interface (right).

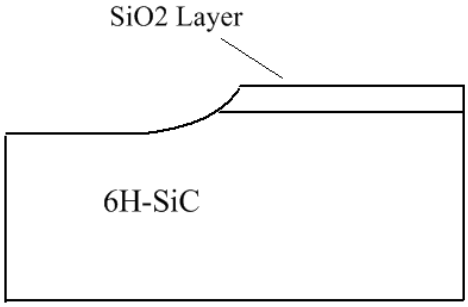

Figure 7. Cross section at the SiC dielectric interface near the electrodes using a concavity.

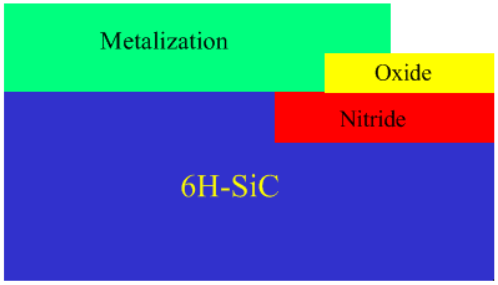

Figure 8. Cross section at the SiC dielectric interface near the electrodes using buried layers.

B. Dielectric Development

One of the DWA objectives is development of the ability to cast the cell module as a fully integrated unit. This objective was realized with the development of high dielectric constant nano-composites made from a polymer resin system and nano-size inorganic particles. The material allows dielectric moldings with complex shapes and effective encapsulation of electrodes and switches. The polymer/particle slurry can be net shape formed into 3-dimensional structures.

In our more recent work, we pursued investigations of the effect of using buried electrodes to minimize enhancement at the triple junction and the scaling of the breakdown electric field for decreased electrode spacing. A typical sample under test is shown in Figure 9. For these tests, we fabricated multiple samples using a matrix of 16 test specimens in a single test sample. In this way we are able assure consistency between each test specimen. The electrodes were polished stainless steel, 2.54 cm diameter with 2 mm spacing.

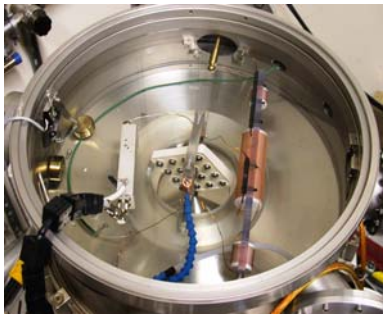

Figure 9. Sample matrix under test.

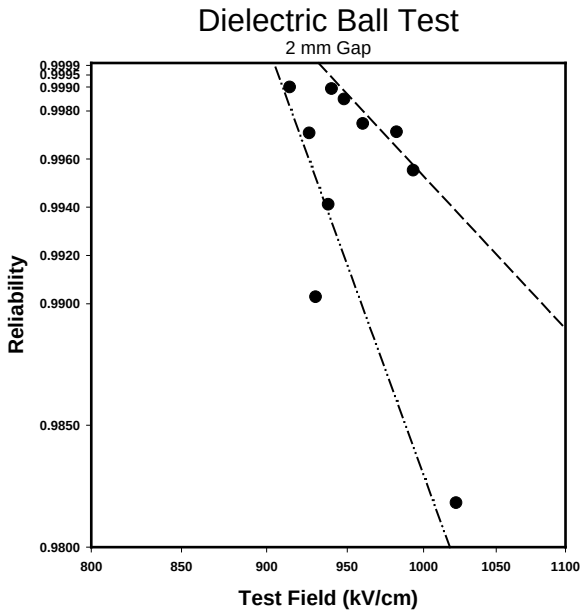

Figure 10. Sample reliability.

Our test on these buried electrode samples determined reliability by subjecting each specimen to multiple pulses at given electric fields. For this test, the electric field is simply the applied voltage divided by gap spacing; the enhancement that results from spherical electrodes is not applied.

Presumably, the cause of failure in these samples is latent partial discharge eventually resulting in complete failure of the sample. What we also observe in this data is the presence of two specific distributions (Fig. 10). The lower distribution of fewer shots on a given sample to achieve breakdown indicates a probable flaw in the material. The upper distribution shows more typical sample behavior. What is evident in this data set is that a

slight reduction in electric field results in significant improvement in reliability: high operational reliability should be achievable at fields approaching ~85 MV/m.

In a separate test, we also attempted to understand the effect of electrode spacing on breakdown electric field. The result of these tests showed an increase from 92 MV/m gradient at the 2 mm spacing to approximately 400 MV/m gradient at approximately 0.1 mm spacing. This latter data used a slow charging waveform at the elevated fields.

C. Multi-layer Insulators

We continue to pursue development of High Gradient Insulators (HGIs) for use as the "dielectric wall" of the DWA. These structures are vacuum insulators composed of alternating layers of metal and dielectric, and have been shown to withstand up to four times the gradient of conventional straight-walled insulators. Although this improvement is similar to that obtained from the standard 45-degree vacuum insulator, the HGI does not have a preferred voltage orientation. This property makes it ideal for applications, like the DWA, where it may be subjected to voltage reversals. Our recent work has shown the important role played by high-voltage conditioning in increasing the flashover threshold of HGIs, and demonstrated improved performance obtained by increasing the dielectric layer thickness. We are also investigating how the displacement current through vacuum insulators may affect dielectric strength under high-gradient, short-pulse conditions.

III. ACCELERATOR CELL TESTS

We recently performed proof of concept cell testing of a DWA cell on ETA-II. Shown in Figure 11 (top) is the downstream beamline of ETA-II with the prototype cell immediately after a transport solenoid. A 60^o analyzing magnet and detector behind the cell was used to determine the added energy gain from the cell under test.

The cell consisted of four separately cast Blumlein structures (τ_p~20 ns) with self-break oil switches initiating the pulse (Fig. 11, lower). Jitter was less than 2 ns. Also shown in the figure are four separate multilayer HGI structures separated by aluminum flanges. This method of assembly was modular which allowed rapid replacement of sections during test. Not shown in the photo are the ferrite isolation cores required to minimize wall currents in the cell housing.

The result of these initial tests are shown in Figure 12. Beam energy measurement as a function of time using a spectrometer is shown. The lower trace is the ETA-II electron beam energy without the DWA cell energized. The upper trace is final beam energy with the DWA cell energized. The net energy gain from this particular data yielded a 3-4 MV/m gradient or approximately one order of magnitude greater than ETA-II.

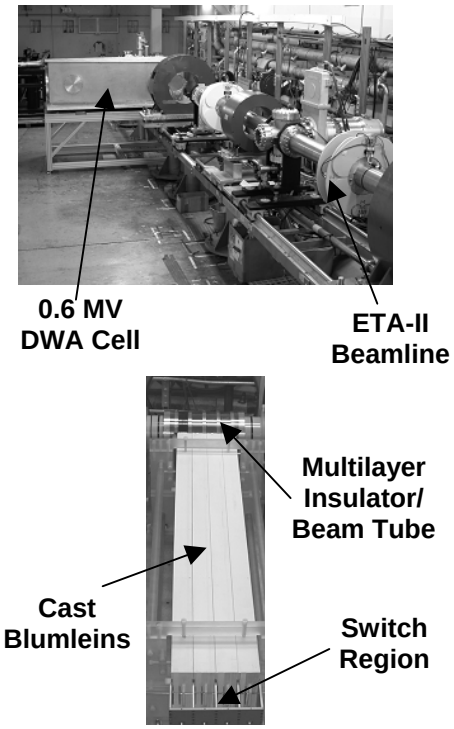

Figure 11. Cast DWA prototype cell during installation (upper photo). Blumleins and insulator structure viewed from the switch end of the structure (lower photo).

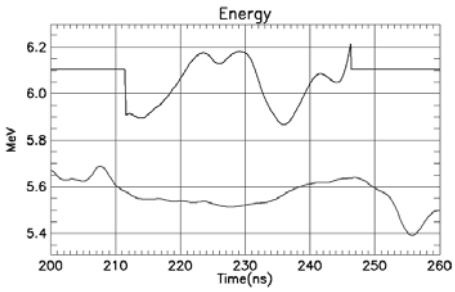

Figure 12. Beam energy measurement as a function of time using spectrometer. Lower trace is ETA-II energy without the DWA cell energized. Upper trace is final beam energy with DWA cell energized.

IV. SUMMARY

We performed component development for a prototype DWA accelerator cell. The cell was tested on ETA-II using a magnetic spectrometer. The gradient achieved during these tests was approximately 3-4 MV/m.

V. ACKNOWLEDGEMENT

*This work was supported under the auspices of the US DOE by Lawrence Livermore National Laboratory under Contract No. DE-AC52-07NA2734.